M–K Ductile Damage Theory Predicts Formability of Stainless Steel Ultra-Thin Strips in Stamping

Tao Fan[1] · Cuirong Liu[1,2] · Yake Wang[1] · Siyuan Liu[1] · Yan Li[1,2]

Abstract

To address the difficulty in forming ultra-thin stainless steel strips, this study focuses on 304 stainless steel ultra-thin strips. By conducting tension and forming limit experiments, the basic mechanical properties and FLC (Forming Limit Curve) of the material are determined, and its formability is systematically investigated. Additionally, to improve testing efficiency and reduce resource consumption, this paper predicts the FLC forming curve of the ultra-thin strip based on the M–K ductile damage model, which is then validated against experimental results, establishing a reliable FLC prediction model. Moreover, to relate it to practical industrial production applications, this study simulates the stamping process of box-shaped components made from the ultra-thin strip based on the theoretical model, exploring the influencing factors of stamping processes on the formability of the ultra-thin strip. The research findings indicate that among the hard, semi-hard, and soft stainless steel ultra-thin strips, the soft one exhibits the best formability, and the 0.05 mm thickness is less formable compared to the 0.1 mm strip. The simulation results demonstrate that the M–K ductile damage theory can reasonably predict the formability of the ultra-thin strip. Furthermore, optimizing the chamfer size in the stamping process, reducing the friction coefficient between the die and the ultra-thin strip, and lowering the stamping speed effectively improve the formability of the ultra-thin strip.

Keywords Stainless steel ultra-thin strip · M–K ductile damage evolution · Forming limit · Stamping forming

1 Introduction

Stainless steel ultra-thin strip, as a new type of precision strip material with a thickness ranging from 0.01 to 0.1 mm, possesses characteristics such as corrosion resistance, high strength, and ease of processing. Due to its excellent decorative and aesthetic properties, it finds wide applications in the fields of electronics, automotive, aerospace, and other industries (Ma et al., 2023). Furthermore, with the advancement of technology, the demand for high-precision, complex-shaped, and lightweight products is increasing across various sectors, leading to a growing interest in stainless steel ultra-thin strip stamping products and related processes.

However, during the stamping process of ultra-thin strips, the material's ductility and damage behavior have a significant impact on the forming results. Especially in the case of stainless steel ultra-thin strip stamping, its high strength and low ductility characteristics make it susceptible to defects such as wrinkles, shearing, and cracking during the stamping process. This presents a significant challenge to the forming quality and production efficiency of stainless steel ultra-thin strip products.

In the research field of stainless steel damage theory, Abdul-Latif et al. (2022) have extensively explored the damage characteristics of 42CrMo steel under varying temperature and strain rate conditions through a combination of uniaxial tension and dynamic compression tests. They

✉ Yan Li
liyy2018023l@163.com

Tao Fan
S202114210084@stu.tyust.edu.cn

Cuirong Liu
ft771132623@163.com

Yake Wang
b202114310006@stu.tyust.edu.cn

Siyuan Liu
2254685906@qq.com

1. School of Material Science and Engineering, Taiyuan University of Science and Technology, Taiyuan 030024, China

2. Preparatory Department, Modern College of Humanities and Sciences, Shanxi Normal University, Linfen 041000, China

also quantitatively analyzed the formation of microcracks and voids using scanning electron microscopy (SEM) and accurately described the flow stress of 42CrMo steel using the Voyiadjis-Abed (VA) constitutive model. Furthermore, Abed et al. (2018) systematically investigated the mechanical properties of EN08 steel within the temperature range of 298–923 K. The experiments revealed that with increasing temperature, the yield strength and ultimate strength of EN08 steel exhibited a decreasing trend, and the strain-hardening characteristics were significantly affected by temperature. They quantified the microcrack and void density in the post-fracture microstructure through SEM image analysis and applied an energy-based damage model to describe the damage evolution process. Subsequently, Abed et al. (2020) studied the thermodynamic response of MMFX steel reinforcement under different temperatures and strain rates through a series of quasi-static and dynamic tests. They employed the Voyiadjis-Abed constitutive model to capture the flow stress characteristics of MMFX steel reinforcement and effectively reproduced the results of room temperature dynamic impact tests through simulation. Additionally, Abed et al. (2017) research also encompassed the flow stress and damage behavior of C45 steel under different temperatures and strain rates. By combining an energy-based damage model with the Johnson–Cook (JC) plasticity model, they successfully predicted the stress–strain response and material softening phenomenon of C45 steel under various conditions. These studies provide a theoretical foundation for understanding and predicting the forming performance of stainless steel materials under different conditions.

However, in the theoretical study of stainless steel forming performance, the Forming Limit Curve (FLC) is one of the most intuitive and effective tools for evaluating the forming performance of metal sheets. It is a curve composed of limit strain points under different deformation paths (Ding et al., 2022; Zhou et al., 2020). During the forming process, if the major and minor strain points of the metal are above the FLC, it is considered that the ultra-thin strip has experienced instability and fracture, otherwise, the metal sheet is in the safe zone. Since obtaining FLC through experiments is a complex process, methods for predicting forming limits based on instability theory have seen significant development.

Marciniak and others (Zdzislaw et al., 1967) proposed a classical material M–K damage constitutive model, which has been widely used to describe the plastic behavior and damage accumulation process of materials. This model, based on plastic anisotropy theory, theoretically analyzes the process of groove formation in sheet metal. Through numerical calculations, the limit strain of the sheet metal is determined as a function of material properties, including initial non-uniformity, strain hardening function exponent, normal anisotropy coefficient, initial plastic strain,

and fracture strain. It can effectively predict the material's deformation, stress distribution, and damage accumulation during the stamping process, providing guidance and theoretical basis for the optimization and improvement of stamping processes. Liu et al. (2019), based on the M–K theory framework and combined with the GTN damage model, developed a new prediction method for the forming limit of high-strength steel 22MnB5. This method introduces correction terms to describe hole aggregation and nucleation of new holes, considers interactions between holes and the material's strain hardening effect, and uses critical hole volume fraction as the instability criterion. By applying theoretical calculations and NAKAZIMA experimental research, the forming limit data of 22MnB5 were obtained and its deformation characteristics were analyzed. The effectiveness of this prediction method was verified through comparison with experimental results. Zheng et al. (2017), based on the M–K theory, derived using the BBC 2005 yield criterion and the Norton-Hoff flow stress model. The BBC 2005 yield criterion describes the material's anisotropic yield behavior through multiple parameters, while the Norton-Hoff model considers the influence of temperature and strain rate on material flow stress. The combined use of these models improves the prediction accuracy of material behavior under complex forming conditions. The research results confirmed the accuracy of the models and indicated that the forming limit curve shifts upward with an increase in these parameters within a certain range of temperature and strain rate, providing a theoretical basis for the optimization of high-temperature forming processes. The introduction of damage models is crucial for accurately simulating the accumulation of internal material damage and failure processes, which is essential for predicting the forming limits of materials.

In summary, for the study of metal forming performance, most scholars have explored the forming performance of stainless steel sheets by optimizing the M–K damage model, but there is limited research on the forming ability of stainless steel ultra-thin strips. Therefore, based on the low ductility characteristics of stainless steel ultra-thin strips, this paper, in addition to the M–K damage model, couples ductility damage during metal forming fracture and uses numerical simulation and experimental verification methods to analyze the forming performance of stainless steel ultra-thin strips. Furthermore, to validate the application of the FLC obtained based on this damage theory and finite element simulation in actual production, this paper takes the forming of stamping box parts as an example. It uses the FLC method to analyze and predict the impact of stamping process parameters on the forming performance of ultra-thin strips, providing a scientific basis for optimizing stamping processes, improving product quality, and extending die life.

2 M–K Ductility Damage Constitutive Model

Micro-mechanical tests of material damage show that the fracture forms of metal forming include ductile fracture, shear fracture, and mixed fracture. According to the existing literature (Li et al., 2018; Zhang et al., 2016; Shahzamanian et al., 2021; Fan et al., 2020), metals experience ductile damage during the stamping process, where plane stress fracture results in localized differences between the metal thickness and the original thickness. Therefore, using ductile damage criteria alone cannot accurately describe the fracture behavior under different loading conditions. This paper combines the two characteristics mentioned above and couples M–K damage with ductile damage to predict the forming limit curve of ultra-thin stainless steel strips.

2.1 M–K Damage Resilience Damage Model Establishment

The M–K damage model describes the phenomenon of localized instability caused by the continuous expansion of inherent defects in quasi-plastic materials under plane stress conditions. (Xiaoxing et al., 2021) It assumes that when defects occur in the material, the sheet will exhibit an uneven thickness distribution. As a result, the damage area is divided into a uniform region A and a thinned groove region B, with thicknesses denoted as t_a and t_b, respectively. The initial geometric defect in the model is defined by the thickness non-uniformity d_0, where d_0 represents the ratio of the thickness between the uniform region A and groove region B. This equation can be expressed using the black metal post-necking thinning rate by Eq. (1), where a_0 is the original thickness, and b_0 is the minimum thickness after sample fracture.

$$d_0 = \frac{t_a}{t_b} = \frac{a_0 - b_0}{a_0} \times 100\% \tag{1}$$

Subsequently, assuming that the groove is perpendicular to the first principal stress direction of the sheet and under the condition of uniaxial strain loading (strain loading condition) with a thickness defect exhibiting anisotropic distribution, accurate predictions of the sheet forming results are achieved by defining an angle function $f_0(\theta)$ for the local material direction. Without considering defects, the stress–strain field within the nominal region is solved, and then each groove is individually considered. Strain compatibility conditions are applied, and the deformation field formulas within each groove, as well as the mechanical equilibrium equations, are calculated separately, as represented by Eq. (2) and (3):

$$\varepsilon_{tt}^A = \varepsilon_{tt}^B \tag{2}$$

$$F_{nn}^B = F, F_{nt}^B = F_{nt}^A \tag{3}$$

In the equation, subscripts n and t respectively represent the directions of the groove normal and tangential to it. F_{nn} and F_{nt} are unit forces in the tangential direction. This numerical term can be used to establish a local damage model for the instability region of the sheet metal, which is used to assess the distribution of thickness changes produced at each unit point.

The ductile damage criterion (Bai et al., 2007) is a phenomenological model commonly used to predict damage caused during forming due to the nucleation, growth, and coalescence of voids inherent in the material. This model assumes that the initial state of damage is a function of equivalent plastic strain $\overline{\varepsilon}_D^{pl}$, stress triaxiality, and strain rate, as given by Eq. (4):

$$\overline{\varepsilon}_D^{pl}\left(\eta, \overline{\varepsilon}^{pl}\right) \tag{4}$$

In the equation, $\eta = p/q$ is the stress triaxiality, where p is the hydrostatic pressure, q is the von Mises equivalent stress, $\overline{\varepsilon}^{pl}$ is the equivalent plastic strain rate, as shown in Eq. (5).

$$\eta = \frac{P}{q} = \frac{(\sigma_1 + \sigma_2 + \sigma_3)/3}{\sqrt{(\sigma_1 - \sigma_2)^2 + (\sigma_2 - \sigma_3)^2 + (\sigma_3 - \sigma_1)^2}/\sqrt{2}} \tag{5}$$

In the equation, σ_1, σ_2 and σ_3 are the principal stresses, and the hydrostatic pressure is represented by Eq. (6).

$$p = (\sigma_1 + \sigma_2 + \sigma_3)/3 \tag{6}$$

The equivalent stress (von Mises stress) is represented by Eq. (7):

$$q = \sqrt{(\sigma_1 - \sigma_2)^2 + (\sigma_2 - \sigma_3)^2 + (\sigma_3 - \sigma_1)^2}/\sqrt{2} \tag{7}$$

(The M–K ductile damage coupled theory model is represented as Fig. S1 in the Figure file.)

2.2 Criterion for Damage Model

When the strain rate in the notch region exceeds a critical value relative to the strain rate in the uniform region, it may lead to the occurrence of local necking instability. Furthermore, when determining the notch position, it becomes impossible to confirm the equilibrium condition value. Based on this, the M–K model assesses the degree of deformation by defining a damage initiation criterion by Eq. (8).

$$F_{eq} = \frac{\Delta \overline{\varepsilon}_B^{pl}}{\Delta \overline{\varepsilon}_A^{pl}}, F_{nn} = \frac{\Delta \varepsilon_{nn}^A}{\Delta \varepsilon_{nn}^B}, F_{nt} = \frac{\Delta \varepsilon_{nt}^A}{\Delta \varepsilon_{nt}^B} \tag{8}$$

In the equation, F_{eq} represents the equivalent unit force, which assesses the degree of deformation in the specified

notch direction and compares it to a critical value. The damage initiation criterion is expressed by Eq. (9).

$$\omega_{mk} = \max\left(\frac{F_{eq}}{F_{eq}^{criy}}, \frac{F_{nn}}{F_{nn}^{criy}}, \frac{F_{nt}}{F_{nt}^{criy}}\right) \tag{9}$$

In the equation, f_{eq}^{criy}, f_{nn}^{criy}, and f_{nt}^{criy} are the critical values of the deformation severity index. Damage initiation occurs when $\omega_{mk} = 1$ or when equilibrium and compatibility equations fail to converge. When $\omega_{mk} = 0$, it is only used to assess the convergence of equilibrium and compatibility equations.

Subsequently, the forming fracture state is determined based on the ductile damage initiation criterion (Morchhale et al., 2021; Zhang et al., 2004), and the initiation criterion is represented by Eq. (10).

$$\omega_D = \int \frac{d\bar{\varepsilon}^{pl}}{\bar{\varepsilon}_D^{pl}\left(\eta, \bar{\varepsilon}^{pl}\right)} = 1 \tag{10}$$

where ω_D is the state variable, which increases monotonically with the plastic deformation. The increment calculation method of ω_D for each increment in the analysis process is represented by Eq. (11).

$$\Delta\omega_D = \frac{\Delta\bar{\varepsilon}^{pl}}{\bar{\varepsilon}_D^{pl}\left(\eta, \bar{\varepsilon}^{pl}\right)} \geq 0 \tag{11}$$

This is used to assess its numerical convergence during predictive calculations.

3 Experimental and Simulation Program Design

3.1 Tensile Test

The experimental material, 304 stainless steel ultra-thin strip, was provided by Shanxi Taigang Stainless Steel Precision Strip Co., Ltd. It has a thickness of 0.1 mm and 0.05 mm (the chemical composition of the stainless steel ultra-thin strip is as indicated in Table S1 in the Table file). The static tensile tests of the 0.1 mm and 0.05 mm thick soft, semi-hard, and hard stainless steel ultra-thin strips were conducted using an electronic universal testing machine controlled by a microcomputer. The tensile strain rate was set at 0.0005 s^{-1}. (The tensile test is represented in Fig. S2 in the Figure file.)

Through tensile tests, stress–strain curves of stainless steel ultra-thin strips with thicknesses of 0.1 mm and 0.05 mm were obtained, as shown in Fig. 1. According to various indicators and the stress–strain curves, it is indicated that the hard state ultra-thin strip first fractures, and the 0.05 mm thick ultra-thin strip shows almost no plastic deformation ability. This phenomenon is related to the material's microstructure and dislocation movement, especially under low strain rates, the Dynamic Strain Aging (DSA) phenomenon may lead to a sudden increase in material strength, thereby reducing the material's plastic deformation ability. In the semi-hard state ultra-thin strip, the elongation of the 0.05 mm thick ultra-thin strip is lower than that of the 0.1 mm thick ultra-thin strip. This indicates that as the thickness decreases, the elongation of the semi-hard state ultra-thin strip also decreases. This trend is related to the Dynamic Strain Aging (DSA) phenomenon, as impurity atoms inside the material may interact with dislocations at low strain rates, increasing the obstacles to dislocation movement,
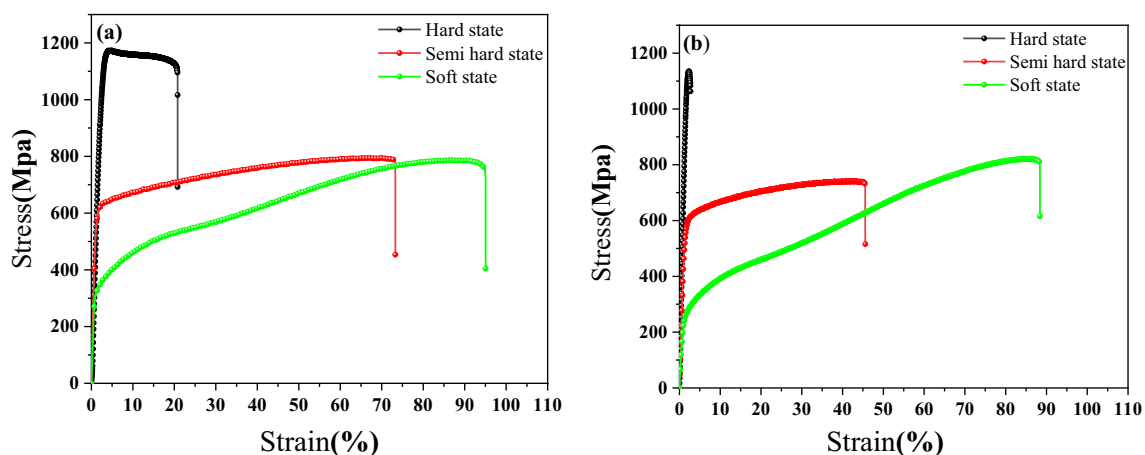

Fig. 1 Tensile fracture curve: **a** 0.1 mm thick tensile fracture curve, **b** 0.05 mm thick tensile fracture curve

thereby affecting the material's plastic deformation ability. Compared to the hard and semi-hard state ultra-thin strips, the soft state ultra-thin strip exhibits higher tensile strain capability, with the elongation of the 0.1 mm and 0.05 mm thick ultra-thin strips being essentially consistent. This result indicates that under soft conditions, the material's plastic deformation ability is superior, which is related to the minor influence of the DSA phenomenon (Hassan & Abed, 2023a, 2023b; Abed et al., 2017). Based on the above tensile test results, this paper selects the soft state ultra-thin strip as the material for forming the specimen, in the hope of avoiding the adverse effects of the DSA phenomenon on the material's performance during the forming process. The various performance indicators of the 304 stainless steel ultra-thin strip are shown in Table 1, providing us with the basic characteristics of the material, which helps us better understand and predict the behavior of the material during the forming process.

3.2 Forming Limit Experiment

According to the national standard GB/T 24171.2–2009 "Determination of Forming Limit Curve of Metal Materials for Sheet and Strip—Part 2: Determination of Laboratory Forming Limit Curve," preparation of stainless steel ultra-thin strip forming samples was done. The deformation widths of the samples were 30 mm, 60 mm, 90 mm, 120 mm, 150 mm, and 180 mm, as shown in Fig. S4. Prior to the forming experiment, the surfaces of the samples were polished using 180# sandpaper and then wiped with alcohol to remove impurities from the surface. Subsequently, within the deformation area, the BLT-A160 laser selective melting equipment from Platinum Force Company was used. The laser power was set to 170W, and a circular grid with a diameter of 2 mm was printed in the deformation area of the forming sample using laser sintering, to monitor the degree of forming distortion of the samples. (The dimensions of the forming specimen and grid are shown in Fig. S3 of the Figure file, and the BLT-A160 laser selective melting equipment from Platinum

Force Company is shown in Fig. S4 of the Figure file. The dimensions of the forming specimen can be found in Table S2 of the Table file.)

The specimens were subjected to hemispherical bulging stamping experiments using a metal sheet forming test machine (as shown in Fig. S5 in the Figure file). In the CNC control panel, the edge pressure was set to 100N, and the stamping speed was set to 0.01 mm/s. Prior to the forming experiment, an appropriate amount of Vaseline lubricant was applied to the deformation area of the specimen facing the convex die to reduce the friction between the sheet and the die, and then the stamping was performed.

In the stamping experiment on stainless steel ultra-thin strips, the observed fractures and forming issues are mainly attributed to several key factors. For deformation paths w = 30 mm, w = 60 mm, w = 90 mm, and w = 120 mm, samples all exhibited path fracture phenomena, especially in the cases of w = 60 mm and w = 90 mm where the depth of the convex features was shallow, and displacement-load data at the convex features were not measured. This phenomenon indicates that during the stamping process, the pressure exerted by the sample is less than the friction between the die and the ultra-thin strip. By adjusting the detection sensitivity of the forming test machine, it was confirmed that excessive friction was the main cause of the fractures. To address this, a significant amount of Vaseline lubricant was applied to the surface of the samples, effectively improving the fracture phenomenon. Further experiments revealed that when the deformation paths increased to w = 150 mm and w = 180 mm, the samples experienced bulging fractures at the convex features. Additionally, wrinkles appeared under the deformation paths of w = 120 mm and w = 150 mm, as shown in Fig. 2a. These defects may be attributed to local stress concentration and uneven deformation of the material during the stamping process. For soft 0.05 mm thick samples, regardless of the deformation width being w = 60 mm or w = 180 mm, the samples directly fractured during the stamping process, as shown in Fig. 2b. Even after adjusting the stamping parameters, it was not possible to optimize their forming state, indicating that the 0.05 mm ultra-thin strip lacks good forming ability under the current stamping conditions. Finally, by interrupting the stamping process at the moment of instantaneous damage to the samples, displacement-load curves of various forming samples of 0.1 mm stainless steel ultra-thin strips were derived. Analysis of these curves revealed that the forming sample with w = 90 mm had the shortest displacement during the stamping deep drawing process, while the forming sample with w = 150 mm exhibited the longest stamping deep drawing displacement, as shown in Fig. 2c. These results reflect the differences in material forming ability and energy consumption during the stamping process under different deformation paths.

Table 1 Tensile properties of 304 stainless steel ultra-thin strip

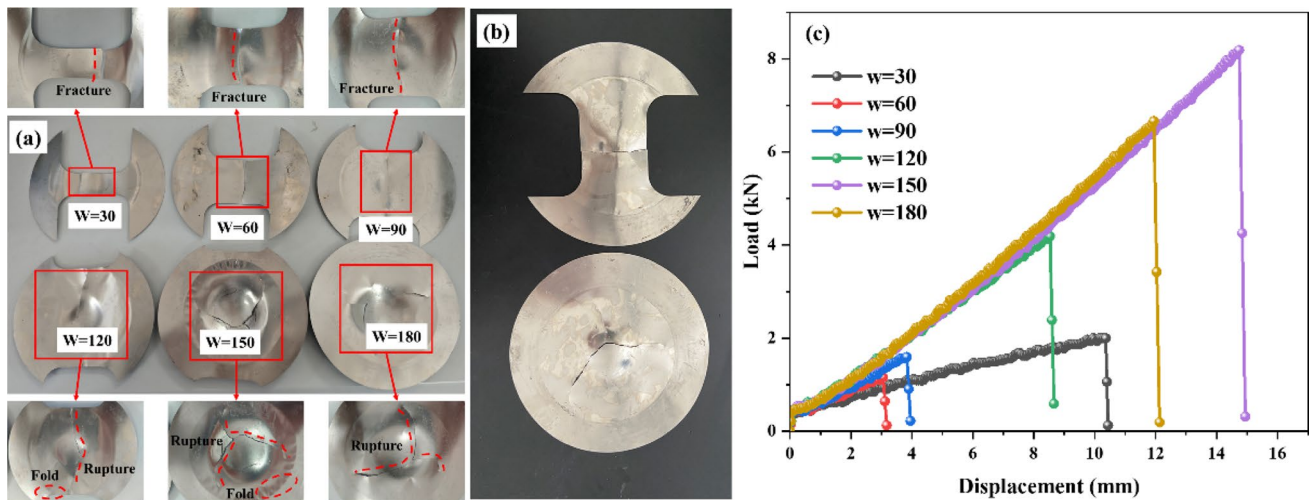| Sample	Elastic modulus (GPa)	Tensile strength (MPa)	Yield strength (MPa)	Yield displacement (mm)
0.1 mm Hard	54.8	1173.0	865.5	1.9
0.1 mm Semi-hard	68.0	793.7	489.4	0.9
0.1 mm Soft	38.3	786.8	310.5	1.0
0.05 mm Hard	72.6	1135.4	1005.3	1.6
0.05 mm Semi-hard	49.3	740.4	508.2	1.2
0.05 mm Soft	26.1	820.7	227.5	1.0

Fig. 2 Stamping results: **a** Stamping results for 0.1 mm thick extreme thin strip, **b** Stamping Results for 0.05 mm thick extreme thin strip, **c** Displacement-load curve with a thickness of 0.1 mm

Label the long axis of the distorted grid circle in the deformation area of the specimen as d_1, and the short axis as d_2, and approximate d_1 and d_2 as the two principal strain directions at a point on the specimen surface (Liu et al., 2017). (The measurement method and the grid distortion form are represented as Fig. S6 in the Figure file.)

Calculate the numerical values of the forming limit points for each test specimen based on the average of the measurement data, as represented by Eq. (12) and (13).

$$\begin{cases} e_1 = \frac{d_1 - d_0}{d_0} \times 100 \\ e_2 = \frac{d_2 - d_0}{d_0} \times 100 \end{cases} \tag{12}$$

$$\begin{cases} \varepsilon_1 = \ln \frac{d_1}{d_0} = \ln\left(1 + e_1\right) \\ \varepsilon_2 = \ln \frac{d_2}{d_0} = \ln\left(1 + e_2\right) \end{cases} \tag{13}$$

In the formula, e_1 represents the major strain in the long-axis engineering, e_2 represents the major strain in the short-axis engineering, ε_1 represents the true major strain in the long axis, and ε_2 represents the true major strain in the short axis. d_1 is the long-axis size after distortion, d_2 is the short-axis size after distortion, and d_0 is the original size of the grid circle. Using strain e_2 (or (ε_2)) as the horizontal axis and e_1 (or ε_1) as the vertical axis, establish a strain coordinate system. Based on the distribution characteristics of strain points in the coordinate system, construct an appropriate curve to obtain the forming limit curve.

3.3 Simulation Model Design

Geometric model and mesh unit division: First, a simulation model was drawn based on the forming test machine's bulging cavity. The material thickness is 0.1 mm, the punch diameter is Φ100 mm, the die and flanging ring outer diameter is Φ180 mm, inner diameter is Φ100 mm, and the die guide fillet is R5. Considering that the flanging ring, die, and punch are not easily deformed during the force process, the constrained model in this model is rigid body, with a contact friction coefficient of 0.3. Since the flanging ring, die, and punch are curved rigid bodies, the mesh in this model is divided using tetrahedral elements and C3D10MT mesh type, making it a 10-node thermal-coupled finite element with hourglass control. For the stainless steel ultra-thin strip, the S4RT mesh type is used in this model to give it hyperbolic thin shell or thick shell element characteristics, followed by its associated M–K ductile damage model characteristics. (The simulation model dimensions and mesh division are shown in Fig. S7 in the attached chart file).

Analysis and solution settings: Studying the displacement forces, temperature, material flow state, etc., of materials with different properties and shapes under various tools and external loads during forming is one of the important issues to be addressed in numerical analysis of material forming processes. Therefore, dynamic explicit Abaqus solver is used in all models, which is suitable for solving complex nonlinear dynamic and quasi-static problems. This module

supports stress/displacement analysis, fully coupled transient temperature/displacement analysis, and acousto-structural coupling analysis. Arbitrary Lagrangian–Eulerian (ALE) adaptive mesh function can effectively simulate large deformation nonlinear problems in the field of material forming.

Post-processing analysis step settings: For stainless steel ultra-thin strips, since the model mesh units are selected as solid elements, in order to observe their forming and damage conditions, it is proposed in the transient analysis module during the output solution in the analysis step: Stress (S) value is used to analyze the stress distribution; Equivalent plastic strain (PEEQ) is used to observe the cumulative results of plastic strain during the deformation process of stainless steel ultra-thin strips; Stiffness degradation scalar (SDEG) and damage initiation criterion (DMICRT) are used to observe the starting variables and damage conditions of the M–K ductile damage model; Failure state (STATUS) is used to automatically delete the mesh units that have completely failed, thereby reducing calculation convergence problems caused by mesh distortion. For overall process output of stainless steel ultra-thin strips, this module needs to select time-displacement (U) and reaction force (RF) to observe the displacement and load-bearing conditions during the stamping process, and can be converted into displacement-load curves to mutually validate with experimental results.

Based on the relevant mechanical performance indicators of the stainless steel ultra-thin strip, including its density, elastic modulus, tensile strength, yield strength, and other parameters, establish the parameters of the damage model. The critical fracture stress value for ductile damage is 786.88 MPa, the triaxial stress intensity η is 0.3, the strain rate is 0.0005 s^{-1}, and the d_0 parameter in the M–K damage model is 0.3 (converted based on the thinning rate of the tensile fracture surface). Since the specimen undergoes uniaxial stress during stamping, the angle θ is set to 90° (material and damage model parameters are shown in Tables S3–S6 in the Table file). Input the above parameters into the material property module of the ABAQUS simulation software. Use these parameters as criteria to evaluate the damage tolerance of the stainless steel ultra-thin strip in the simulation software, and set them in the mesh module. When the applied load exceeds the mechanical performance indicators mentioned above, automatically delete the mesh elements that exceed the upper limit, thus exhibiting damage phenomena similar to experimental results.

3.4 Result Analysis

According to the M–K ductile damage theory, during the forming fracture of the metal ultra-thin strip, localized thinning occurs, resulting in ductile damage. (Taking the specimen with a deformation width of 30 mm as an example, the simulated

cloud map of the forming fracture is shown in Fig. S8 in the Figure file. The two blue and red areas in the view represent the thinning areas A and B in the M–K model. The ductile damage phenomenon of the metal is deduced based on the simulated fracture surface, which corresponds to the experimental fracture phenomenon of the ultra-thin strip.)

To accurately fit the experimental FLC, this study divides the simulation results into critical instability states and damage fracture states, as shown in Fig. 3. Select the node with the deepest displacement in the chosen critical instability state simulation model, export the history output data of its reaction force (RF) and displacement (U), plot the displacement-load curve (as shown in Fig. S9 in the Figure file), to compare and verify it against experimental results, exploring the feasibility of the simulation predictions. It is found that for the simulation results of deformation paths w = 30 mm, 60 mm, 90 mm, and 120 mm, both the displacement and load are greater than the experimental data. For the simulation results of deformation paths w = 150 mm and 180 mm, the load is greater than the experimental data, but the displacement is smaller than the experimental data. Additionally, in the experimental data, there is a certain linear increasing trend in the initial load. This is because the material of the stainless steel ultra-thin strip is soft. When the die just contacts the stainless steel ultra-thin strip, there will be a certain amount of sinking, causing the forming test machine to detect a large span of load in a very small displacement range. Subsequently, the load and displacement exhibit a certain linear trend. The simulation data tend to be idealized, showing a linear trend from the origin to the point of rupture of the stainless steel ultra-thin strip. These observations indicate that there is a certain deviation between the simulation data and the experimental results, but overall, the fitting degree is high, indicating that predicting the stamping forming performance of stainless steel ultra-thin strips based on the M–K damage model is feasible.

By selecting the grid points at the deformation area of the specimens in the critical instability state, primary and secondary strain values are obtained, and the FLC is then plotted and validated against the experimental results. The forming limit diagram is shown in Fig. 4. After performing a nonlinear fit to the forming limit points, the curve error between simulation and experiments is 5%, confirming the predictability of the M–K ductile damage model for the forming ability of extremely thin strips.

4 Influence Factors on the Forming of Extremely Thin Strips Stamping Box Components

To verify the practical application of this model in industrial production, this study analyzed the forming effect of a 200 mm * 200 mm * 0.1 mm stainless steel ultra-thin
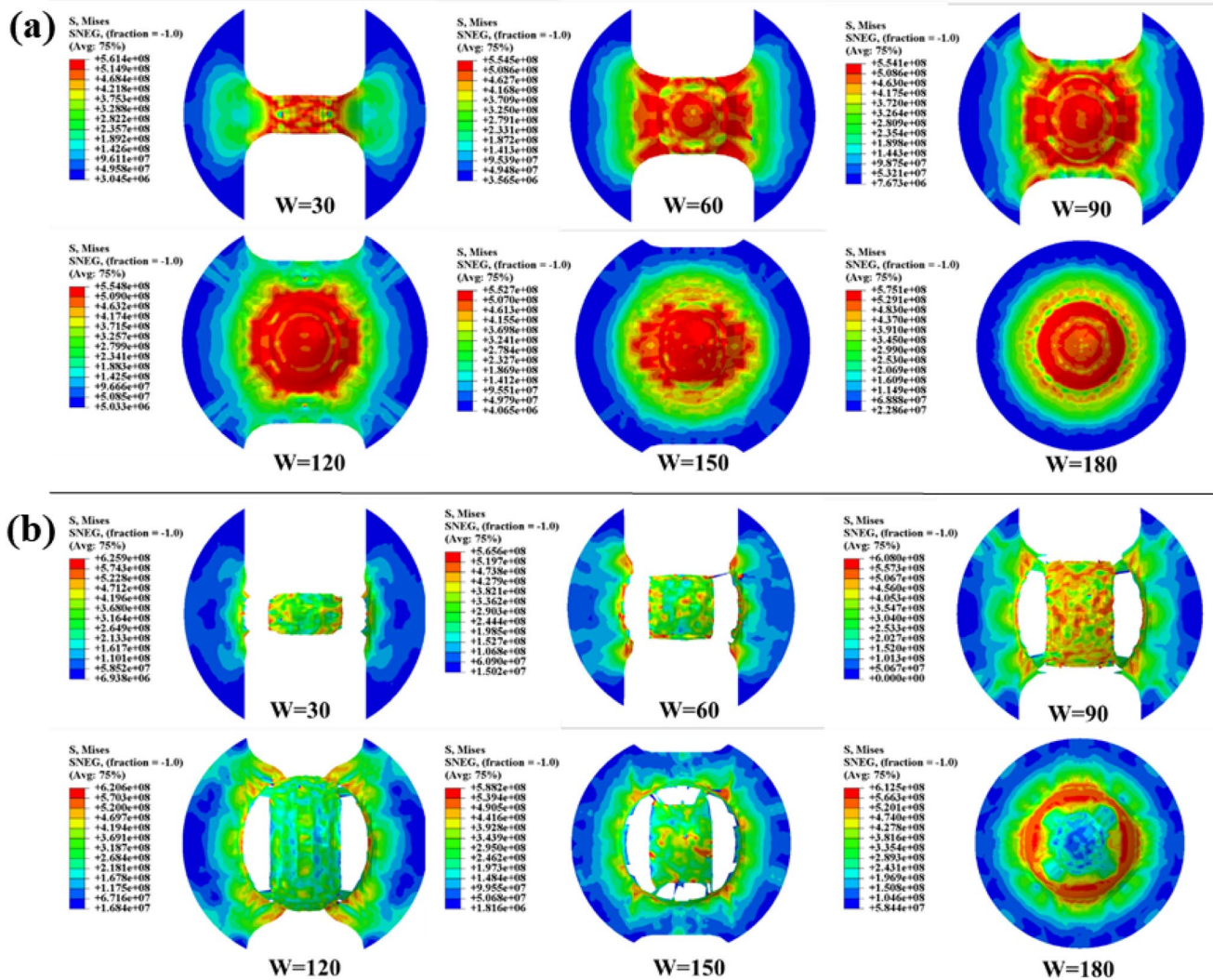
Fig. 3 Damage condition: **a** critical damage state of the formed specimen; **b** damage and rupture state of the formed specimen

strip when stamping square box parts based on the experimental data and the FLC of the stainless steel ultra-thin strip. The analysis focused on the stamping deep drawing and edge pressing areas of the box parts. By changing the friction coefficient between the die and the sheet metal, the die chamfer size, and the punch speed during the stamping process, the study aimed to investigate the forming impact of different process parameters on the deep drawing region of the stainless steel ultra-thin strip square box parts. (A schematic illustration of the damage analysis is shown in Fig. S10 in the Figure file.)

4.1 Influence of Mold Fillet on the Formability of Extremely Thin Belt-Boxed Parts

With a planned stamping speed of 0.1 mm/s and a contact friction coefficient of 0.35, different fillet radii (R) of 5, 10,

and 15 are set to investigate their impact on the formability of 0.1 mm soft stainless steel belts. The main and minor strain values in the deep drawing region of the thin belt are selected and mapped onto the FLC chart as shown in Fig. 5.

The main and minor strain values in the deep drawing region are distributed above and below the FLC. Points in the deep drawing and edge-pressing region of the boxed part are evenly distributed within the forming safety zone, while the deep drawing damage zone of the boxed part is distributed within the instability zone. When the fillet radius is R5, the deep drawing damage zone is close to the forming boundary safety zone, and the mapped points are relatively concentrated, indicating that in the stamping process, the deep drawing region of the boxed part is subjected to external pressure or bending stress, leading to stress concentration in this area, thus increasing the risk of cracking or fracture of the boxed part, as shown
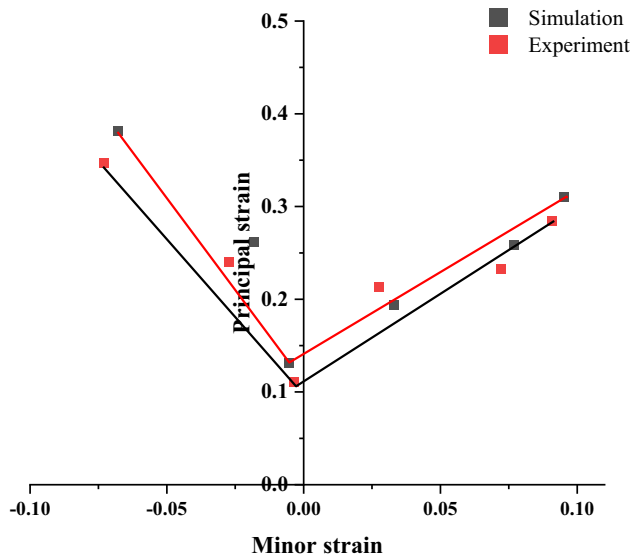
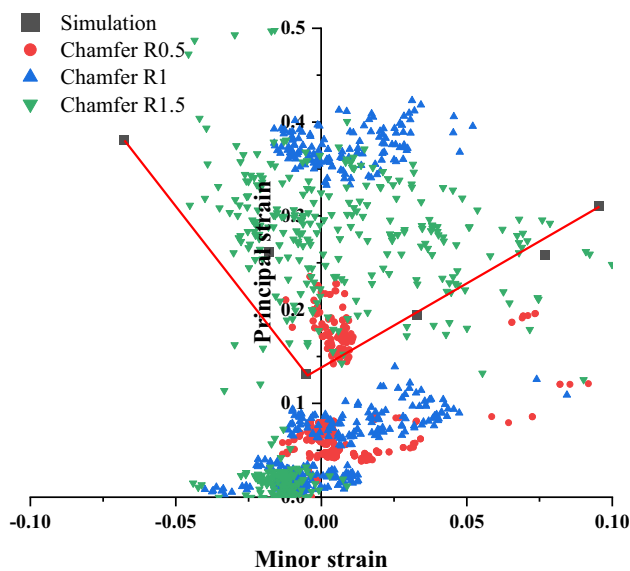**Fig. 4** Simulation curve of forming limit experiment

Fig. 5 FLC plot of primary/secondary strain value mapping of grids with different chamfered pull-down areas

in Fig. 6a. When the fillet radius is increased to R10, the mapped points of the deep drawing damage zone are more scattered, but compared to R5, they are farther from the forming safety boundary, indicating that increasing the fillet radius can effectively improve the formability of the extremely thin belt. Increasing the fillet radius to R15, both the deep drawing and edge-pressing regions, as well as the deep drawing damage zone, are farther from the forming safety boundary. This is because when the fillet radius is increased, it improves the formability of the

extremely thin belt in the mold during stamping, reducing flow resistance and shear forces (Chen et al., 2003; Yang al., 2017), thereby reducing resistance during the feeding process of the extremely thin belt and enabling a smoother completion of the stamping forming process, as shown in the simulation forming diagram in Fig. 6c.

4.2 Influence of Mold Contact Friction Coefficient on the Formability of Extremely Thin Belt-Boxed Parts

With a planned stamping speed of 0.1 mm/s and a fillet radius of R10, different contact friction coefficients between stainless steel extremely thin belts and the mold are set to 0.35, 0.25, and 0.1, respectively, to investigate their impact on the formability of 0.1 mm soft stainless steel extremely thin belts. The main and minor strain values in the deep drawing region of the extremely thin belt are selected and mapped onto the FLC chart, as shown in Fig. 7.

In the FLC, the principal and minor strains of the deep drawing area are distributed above and below. The points in the edge pressing area of the box part are evenly distributed in the forming safety zone, while the damage zone of the deep drawing in the box part is evenly distributed in the unstable area. Under different contact friction coefficients, the distribution of principal and minor strains in the edge pressing area of the deep drawing is more concentrated, indicating that the edge pressing area is almost unaffected by the friction coefficient process parameters. However, the damage zone of the deep drawing gradually moves away from the FLC as the friction coefficient increases, indicating that the forming ability of the box part gradually deteriorates. This is because the friction coefficient directly affects the filling performance of the extremely thin strip in the die. A larger friction coefficient will hinder the filling of the extremely thin strip during stamping, resulting in incomplete filling or deviation in the forming area of the die. It may also lead to the generation of frictional heat, increasing the heat at the contact between the die and the sheet metal, thereby increasing surface thermal deformation and burrs (Zhao al., 2023). A smaller friction coefficient helps reduce surface defects and improve surface quality, as shown in Fig. 8.

4.3 The Impact of Mold Contact Friction Coefficient on the Formability of Ultra-Thin Sheet Metal Box Parts

A stamping speed of 0.1 mm/s and a fillet radius of R10 are proposed. Different contact friction coefficients between the stainless steel ultra-thin sheet and the mold are set to 0.35, 0.25, and 0.1, respectively, to investigate their influence on the formability of 0.1 mm soft stainless steel ultra-thin
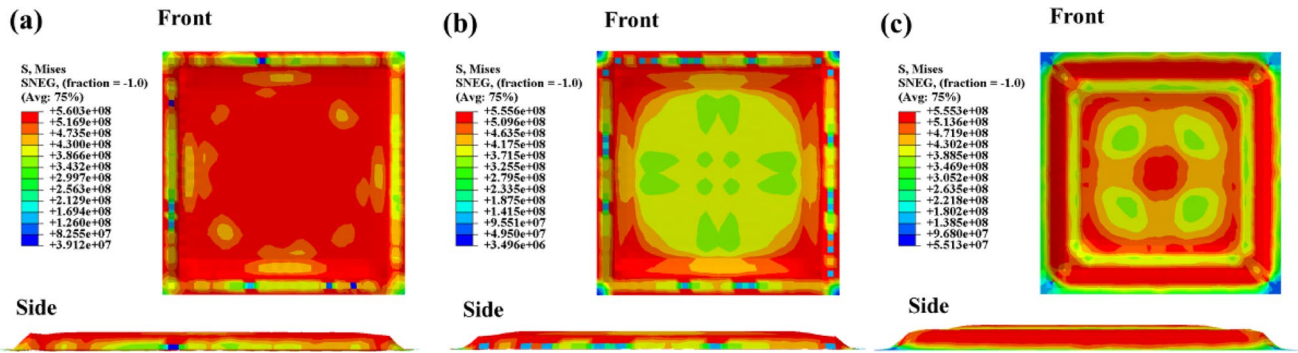
Fig. 6 The stamping simulation results of the box under different chamfer sizes are: **a** chamfer R5, **b** chamfer R10, **c** chamfer 15
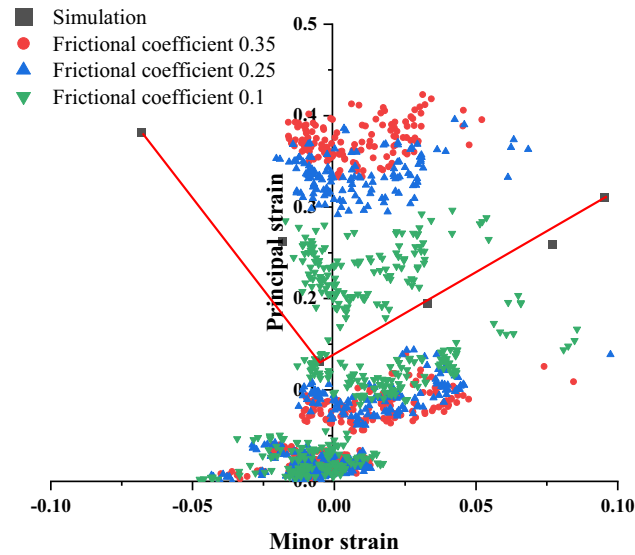

Fig. 7 FLC plot of primary/secondary strain value mapping of grids with different contact friction coefficients under the pull-down region

sheets. The main/minor strain values in the ultra-thin sheet stamping deep-drawing region are selected and mapped onto the FLC chart, as shown in Fig. 9.

The major/minor strain values in the deep-drawing area are distributed above and below the FLC, and the points in the flange's deep-drawing and flanging areas are evenly distributed within the forming safety zone. When the punch stamping speed is 0.1 mm/s and 0.05 mm/s, the deep-drawing damage zone in the flange area is evenly distributed in the unstable region. When the punch stamping speed is 0.01 mm/s, the deep-drawing damage zone is evenly distributed in the safe region.

Based on the distribution of major and minor strain index values in the deep-drawing area, it can be observed that the punch speed has a relatively small impact on the flanging area of the deep-drawing zone, indicating that the flanging area is almost unaffected by the punch stamping process parameters. For the deep-drawing damage zone, when the punch speed is 0.1 mm/s, the mapped points are farthest from the FLC boundary. When the punch speed is 0.05 mm/s, the major and minor strain index mapping points are distributed at the FLC boundary. When the punch speed is 0.01 mm/s, the major and minor strain index mapping points are in the safe zone of the FLC, indicating that reducing the punch stamping speed can effectively improve the forming ability of the box-shaped part.
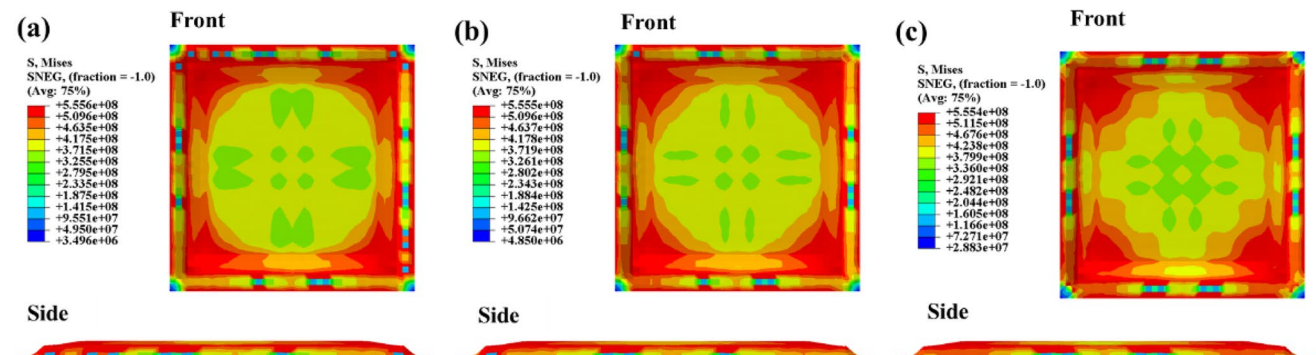

Fig. 8 The stamping simulation results of box parts under different contact friction coefficients are: **a** friction coefficient 0.35, **b** friction coefficient 0.25, **c** friction coefficient 0.1
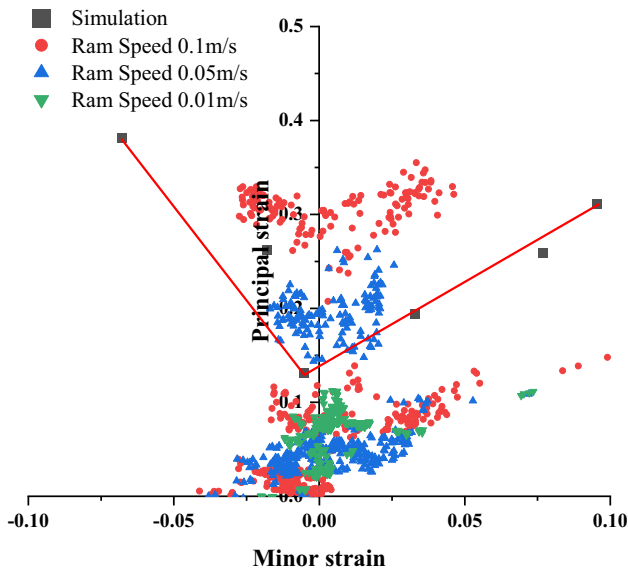
Fig. 9 FLC diagram of the map of primary/secondary strain values in the grid of the pull-down area at different stamping speed

This is because as the punch speed decreases, the flow resistance of the ultra-thin strip in the die decreases, making it less prone to damage such as squeezing and tearing during stamping, and improving the forming accuracy of the ultra-thin strip. The punch speed also affects the surface quality of the box-shaped part. High-speed stamping increases the friction between the material and the die, leading to frictional heat and surface defects such as scratches and wear, reducing the surface quality of the ultra-thin strip material, as shown in Fig. 10.

Compared to sheet metal, ultra-thin strips have lower strength and toughness, and excessive punch speed can lead to unpredictable forming behavior for stainless steel ultra-thin strips. Irregular bulges may appear on the surface of the ultra-thin strip, reducing the precision of forming the box-shaped part, as shown in Fig. 10a.

5 Conclusion

(1) Tensile and formability tests were conducted on ultra-thin stainless steel strips of different hardness grades. By comparing the soft ultra-thin stainless steel strip with other hardness grades of ultra-thin strips, each 0.1 mm thick, we found that the soft strip exhibited stronger formability. Additionally, for ultra-thin strips with thicknesses below 0.05 mm, a significant decrease in formability was observed, making effective forming nearly impossible. To validate these findings, a series of experimental tests were carried out, with at least 5 repetitions under each condition to ensure the reliability and statistical significance of the data.

(2) The application of the M–K ductile damage model in simulation can reasonably predict the state of instability and rupture of stamped stainless steel extremely thin strips. By obtaining the average values of primary and secondary strains of simulated rupture mesh points to plot the FLC, it can be mutually verified with the experimentally derived FLC.

(3) Optimizing the die chamfer size, reducing the friction coefficient between the die and the extremely thin strip, and decreasing the stamping speed during the stamping process can enhance the forming ability of stainless steel extremely thin strips. However, in actual production processes, the rational selection and optimization of parameters should be based on the specific material and thickness of the extremely thin strips to achieve the best forming results.
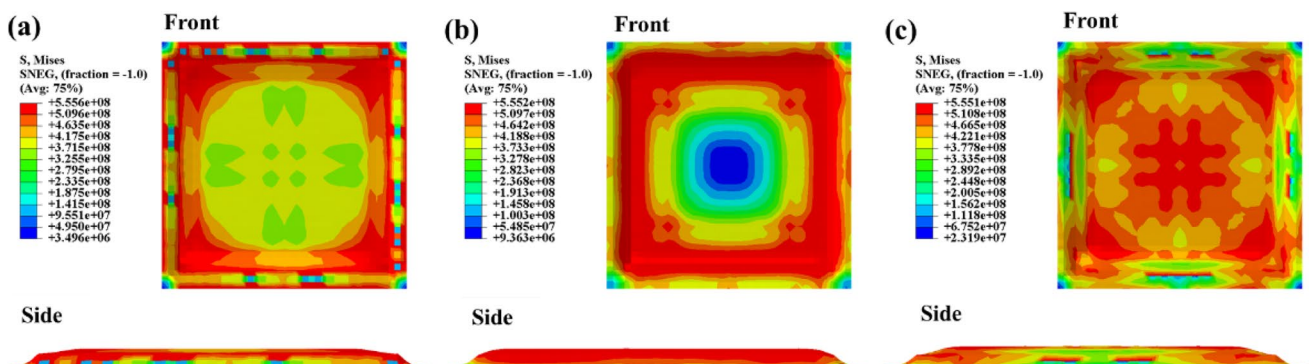

Fig. 10 The stamping simulation results of box parts under different stamping speeds: **a** stamping speed 0.1 mm/s, **b** stamping speed 0.05 mm/s, **c** stamping speed 0.01 mm/s

Data Availability The datasets generated during and/or analyzed during the current study are available from the corresponding author on reasonable request.

Declarations

Conflict of interest There are no conflict to declare.

References

Abdul-Latif, A., Abed, F., Oucif, C. H., & Voyiadjis, G. Z. (2022). Effect of various temperatures and strain-rates combinations on the thermomechanical behavior of 42CrMo steel. *Archives of Mechanics, 74*(5), 345–372.

Abed, F., Abdul-Latif, A., & Voyiadjis, G. Z. (2020). Performance of MMFX Steel Rebar at Elevated Temperatures. *Journal of Engineering Mechanics, 146*(11), 04020126.

Abed, F., Abdul-Latif, A., & Yehia, A. (2018). Experimental Study on the Mechanical Behavior of EN08 Steel at Different Temperatures and Strain Rates. *Metals, 8*(9), 736.

Abed, F. H., Saffarini, M. H., Abdul-Latif, A., & Voyiadjis, G. Z. (2017). Flow Stress and Damage Behavior of C45 Steel Over a Range of Temperatures and Loading Rates. *Journal of Engineering Materials and Technology, 139*, 021012-1–021012-8.

Bai, Y., & Wierzbicki, T. (2007). A new model of metal plasticity and fracture with pressure and Lode dependence. *International Journal of Plasticity, 24*(6), 1071–1096.

Chen, X., & Jiang, H. (2003). Prediction and verification of forming limit diagram in the flanging zone of automotive steel sheet. *Metal Forming Technology, 21*(06), 86–88.

Ding, H., Pan, J., Wan, J., et al. (2022). Influence of GTN damage parameters on the forming limit curve of DP780 steel sheet. *Journal of Plasticity Engineering, 4*, 151–157.

Fan, W. (2020). *Research on the micromechanical behavior of deformation zone in 304 stainless steel ultra-thin strip rolling*. Taiyuan University of Technology.

Hassan, A., & Abed, F. (2023a). Constitutive modeling of thermomechanical abnormalities due to dynamic strain aging in commercially pure titanium. *Journal of Materials Research and Technology, 25*, 5174–5183.

Hassan, A., & Abed, F. (2023). Constitutive modeling of dynamic strain aging in commercially pure bcc metals. *Mechanics of Advanced Materials and Structures*. https://doi.org/10.1080/15376494.2023.2236616

Li, W., Zhou, T., Liao, F., et al. (2018). Application of ductile damage criteria in dynamic time history analysis of steel frame structures. *Building Structure, 22*, 21–27.

Liu, D., Xu, G., & Chang, C. (2017). Forming limit diagram and its calculation model for DP780 high-strength steel sheet in warm forming. *Journal of Plasticity Engineering, 24*(02), 192–197.

Liu, W., Ying, L., Rong, H., et al. (2019). Prediction of forming limit of high-strength steel based on modified M–K model. *Journal of Jilin University: Engineering and Technology Edition, 4*, 1266–1271.

Ma, W., Guan, H., Zhang, X., et al. (2023). Preparation process and bending performance study of carbon fiber/stainless steel ultra-thin fiber metal laminates. *Journal of Composite Materials, 2023*, 1–12.

Morchhale, A., Badrish, A., Kotkunde, N., et al. (2021). Prediction of fracture limit of Ni–Cr based alloy under warm forming conditions using ductile damage model and numerical methods. *Transactions of Nonferrous Metals Society of China, 31*(08), 2372–2387.

Shahzamanian, M. M., & Wu, D. P. (2021). Study of forming limit diagram (FLD) prediction of anisotropic sheet metals using Gurson model in M–K method. *International Journal of Material Forming, 14*(5), 1031–1041.

Xiaoxing, L., Yangkai, C., Lihui, L., et al. (2021). A modified M–K method for accurate prediction of forming limit curve of aluminum alloy. *Metals, 11*(3), 1031–1041.

Yang, X. (2017). *Study on prediction of forming limit in hot stamping of high-strength steel TRB box parts*. Harbin Institute of Technology.

Zdzislaw, M., & Kazimierz, K. (1967). Limit strains in the processes of stretch-forming sheet metal. *International Journal of Mechanical Sciences, 9*(9), 3–394.

Zhang, X., Liu, C., Zheng, Y., et al. (2016). Prediction of forming limit of aluminum alloy based on ductile damage and shear damage. *Journal of Jilin University: Engineering and Technology Edition, 5*, 1558–1566.

Zhang, Z. (2004). Numerical simulation of tensile fracture of ductile metal cylindrical bar. *Journal of Plasticity Engineering, 03*, 11–14.

Zhao, F., Cheng, X., Gao, Z., et al. (2023). Influence of mold parameters on the forming damage value of SS316L stainless steel bipolar plate step-type flow channel. *Journal of Plasticity Engineering, 8*, 49–56.

Zheng, X., & Chen, J. (2017). Prediction and analysis of high-temperature forming limit based on M–K theory. *Die & Mould Industry, 6*, 1–6.

Zhou, P., Zhu, R., Shi, C., et al. (2020). GTN model-based damage modeling for warm forming of 5A06 aluminum alloy. *Journal of Plasticity Engineering, 12*, 164–169.